Redox Biology 14 (2018) 261–271

Contents lists available at ScienceDirect

Redox Biology

journal homepage: www.elsevier.com/locate/redox

Research Paper

Cardiac-specific inactivation of LPP3 in mice leads to myocardial dysfunction and heart failure

Mini Chandra[a], Diana Escalante-Alcalde[b], Md. Shenuarin Bhuiyan[c], Anthony Wayne Orr[c], Christopher Kevil[c], Andrew J. Morris[d], Hyung Nam[e], Paari Dominic[f], Kevin J. McCarthy[a,c], Sumitra Miriyala[a,*], Manikandan Panchatcharam[a,*]

[a] Department of Cellular Biology and Anatomy, Louisiana State University Health Sciences Center, Shreveport, USA
[b] División de Neurociencias, Instituto de Fisiología Celular, Universidad Nacional Autónoma de México, México DF, Mexico
[c] Department of Pathology and Translational Pathobiology, Louisiana State University Health Sciences Center, Shreveport, USA
[d] Division of Cardiovascular Medicine, University of Kentucky, Lexington, USA
[e] Department of Pharmacology and Toxicology, Louisiana State University Health Sciences Center, Shreveport, USA
[f] Division of Cardiology, Department of Medicine, Louisiana State University Health Sciences Center, Shreveport, USA

ARTICLE INFO

Keywords:
Heart failure
Lipid phosphate phosphatase
Lysophosphatidic acid

ABSTRACT

Lipid Phosphate phosphatase 3 (LPP3), encoded by the *Plpp3 gene,* is an enzyme that dephosphorylates the bioactive lipid mediator lysophosphatidic acid (LPA). To study the role of LPP3 in the myocardium, we generated a cardiac specific *Plpp3* deficient mouse strain. Although these mice were viable at birth in contrast to global *Plpp3* knockout mice, they showed increased mortality ~ 8 months. LPP3 deficient mice had enlarged hearts with reduced left ventricular performance as seen by echocardiography. Cardiac specific *Plpp3* deficient mice had longer ventricular effective refractory periods compared to their *Plpp3* littermates. We observed that lack of Lpp3 enhanced cardiomyocyte hypertrophy based on analysis of cell surface area. We found that lack of Lpp3 signaling was mediated through the activation of Rho and phospho-ERK pathways. There are increased levels of fetal genes Natriuretic Peptide A and B (*Nppa* and *Nppb*) expression indicating myocardial dysfunction. These mice also demonstrate mitochondrial dysfunction as evidenced by a significant decrease ($P < 0.001$) in the basal oxygen consumption rate, mitochondrial ATP production, and spare respiratory capacity as measured through mitochondrial bioenergetics. Histology and transmission electron microscopy of these hearts showed disrupted sarcomere organization and intercalated disc, with a prominent disruption of the cristae and vacuole formation in the mitochondria. Our findings suggest that LPA/LPP3-signaling nexus plays an important role in normal function of cardiomyocytes.

1. Introduction

The phospholipid phosphatase 3 (*PLPP3*) gene encodes LPP3, an integral membrane protein which is Mg^{2+}-independent and N-ethylmaleimide insensitive enzyme responsible for the dephosphorylation of lipid phosphates such as phosphatidic acid (PA) and lysophosphatidic acid (LPA). It is robustly expressed in the heart [1]. Subcellularly, LPP3 is located in the plasma membrane [2], the endoplasmic reticulum (ER), Golgi complex and endosomes [3,4]. Global knockout of *Plpp3* (formerly *Ppap2b*) in mice leads to embryonic lethality around embryonic age 10 due to defects in the development of extraembryonic vasculature [5]. In addition, we have demonstrated that deficiency of endothelial cell specific LPP3 leads to increased vascular permeability and defective cardiovascular development resulting in embryonic lethality [6] and knockout of *Plpp3* in both endothelial or smooth muscle cells shows enhanced inflammation and permeability [6,7]. These findings imply that LPP3 expression is essential for normal prenatal cardiovascular development and, in adult mice, LPP3 normally functions to maintain the vascular integrity and attenuate inflammation.

Although other functions are likely, LPP3 is a key regulator of the bioactive lipid LPA and terminates its signaling function through dephosphorylation. LPA plays a well-known role in atherosclerotic disease. A six-fold increase in serum LPA concentration has been observed following acute myocardial infarction in patients (1.66 mg/L vs 10.43 mg/L, $P < 0.001$) [8]. We have shown that exogenous

Abbreviations: Plpp3, Phospholipid phosphatase 3; LPA, lysophosphatidic acid; PA, phosphatidic acid

* Corresponding authors.
E-mail addresses: smiriy@lsuhsc.edu (S. Miriyala), mpanch@lsuhsc.edu (M. Panchatcharam).

http://dx.doi.org/10.1016/j.redox.2017.09.015
Received 29 August 2017; Received in revised form 15 September 2017; Accepted 19 September 2017
Available online 28 September 2017

administration of LPA increases heart rate and left ventricular pressure in vivo [9]. Furthermore, LPA has been shown to induce cardiomyocyte hypertrophy in cell culture models [10,11]. These findings suggest a critical role for LPA-mediated signaling in the myocardium. Interruption of LPA signaling in the myocardium may be an important factor in protecting the heart against insult and injury. As conventional deletion of the *Plpp3* results in severe embryonic developmental abnormalities [5], a specific role for the LPP3 enzyme in adult myocardium remains unknown. Therefore, we used the Cre/*loxP* system to delete *Plpp3* specifically in cardiomyocytes. This strategy resulted in mice which do not express LPP3 in the heart. Here, we characterize these animals in order to understand the role of LPP3 in the adult myocardium under physiological conditions. Our findings indicate that LPP3 serves as an intrinsic negative regulator of LPA mediated cardiomyocyte hypertrophy. These findings suggest that LPP3 is crucial in maintaining the normal cardiac homeostasis and plays an important role in the protection of cardiomyocytes in vivo.

2. Material and methods

2.1. Generation of mice with cardiac-specific deletion of Plpp3

The production and initial characterization of mice carrying a conditional allele of *Plpp3* (*Plpp3*^{fl}) have previously been described [6,7]. *Plpp3*^{fl} mice were backcrossed for > 10 generations into the C57Bl/6 background. These mice were then crossed with C57Bl/6 mice expressing Cre recombinase under the control of the cardiac-specific alpha-myosin heavy chain promoter (*Myh6-Cre*) [12] to obtain congenic *Plpp3*$^{\Delta}$ mice.

The mice survived in the expected numbers. Mating of homozygous *Plpp3*^{fl} with *Plpp3*$^{\Delta}$ mice yielded 50% *Plpp3*$^{\Delta}$ offspring with less than 2% mortality at birth. Mice were housed in cages with HEPA-filtered air in rooms on 12-h light cycles and fed Purina 5058 rodent chow ad libitum. Systolic blood pressure and heart rate were measured for five consecutive days noninvasively in conscious mice using the CODA blood pressure analysis tail-cuff system (Kent Scientific Corporation, Torrington, CT) daily after training for one week. All procedures conformed to the recommendations of Guide for the Care and Use of Laboratory Animals (Department of Health, Education, and Welfare publication number NIH 78-23, 1996), and were approved by the Institutional Animal Care and Use Committee. Neonatal cardiomyocytes were isolated from the *Plpp3*^{fl} with *Plpp3*$^{\Delta}$ mice as described previously [13] (Supplementary video shows the beating neonatal cardiomyocyte derived from *Plpp3*^{fl} mice).

Supplementary material related to this article can be found online at http://dx.doi.org/10.1016/j.redox.2017.09.015.

2.2. Echocardiography

Transthoracic echocardiography was performed on male 8-month-old, using a 30 MHz probe and the Vevo 3100 Ultrasonograph (VisualSonics). Mice were lightly anesthetized with 0.8% isoflurane, maintaining the heart rate at 400–500 beats/min. The hair was removed from the chest using a chemical hair remover (Nair®). The heart rate and body temperature were maintained and recorded. Sonographers were blinded as to genotypes being analyzed. Two-dimensional directed M-mode echocardiographic images along the parasternal short axis were recorded to determine left ventricular (LV) size and systolic function. M-mode measurements included the LV internal dimensions in systole and diastole (LVIDs and LVIDd, respectively) as well as the diastolic thickness LV posterior wall (LVPWd) and the diastolic interventricular septum thickness (IVSd). Percent fraction shortening was calculated as [(LVIDd − LVIDs)/LVIDd] × 100 [14].

2.3. ECGs and electrophysiology studies

Surface resting ECGs and electrophysiology studies were performed on male 12-week-old Plpp3$^{\Delta}$ mice and compared with those in an age-matched group of adult male Plpp3^{fl} control mice. Mice were anesthetized with isoflurane (2% for induction and 1.5% for maintenance of anesthesia; Apollo Tech 3 Vaporizer; NorVap). During EP studies the mouse body temperature was monitored by an intra-rectal probe and controlled using mouse pad circuit board equipped with a heating element (Rodent Surgical Monitor, Indus Instruments, USA). All studies were performed at 37.0 ± 0.5 °C. We used a Millar 1.1F octapolar EP catheter (EPR-800; Millar Instruments) inserted via a cut down of the internal right jugular vein. The catheter was advanced to the right atrium and ventricle using electrogram guidance and pacing capture to verify intracardiac position. A computer-based data acquisition system (PowerLab 16/30; ADI Instruments) was used to record a 1-lead body surface ECG and up to 4 intracardiac bipolar electrograms (LabChart Pro software, version 7; AD Instruments). In brief, the right ventricular pacing was performed using 2 ms current pulses delivered by an external stimulator (STG-3008 FA; Multi Channel Systems). Ventricular effective refractory period (VERP) or ventricular tissue refractoriness and ventricular arrhythmia inducibility were assessed by single extra stimulation or burst pacing using an automated stimulator. To determine VERP, the single ventricular extra stimulus was placed at a pacing drive of 100 ms. A drive train of eight paced beats (S1 × 8) followed by delivery of a single extra stimulus (S2) was given until ventricular stimuli failed to result in ventricular depolarization. To induce ventricular tachycardia, the triple extra stimulation technique was utilized first. Triple extra stimuli were delivered with S2, S3 or S4 extra stimuli brought down to a minimum coupling interval of 30 ms (1). If this maneuver failed to induce ventricular tachycardia (VT), we then performed burst pacing. Burst pacing started at a 40 ms cycle length, decreasing by 2 ms every 2 s to a cycle length of 20 ms. Burst pacing was repeated one minute after the previous burst concluded or the termination of VT. If the mice were non-inducible for VT, we then repeated the above maneuvers after an IP injection of Isoproterenol (1 ng/g). Ventricular tachycardia was defined as 4 consecutive beats of ventricular premature depolarizations or more [15].

2.4. RNA isolation and quantitative PCR

Human and mouse Plpp3 lentiviruses were derived as described previously [7]. Total RNA was extracted from heart tissues and primary cardiomyocytes using the RNeasy mini kit (Qiagen, Chatsworth, CA) following manufacturer's instructions. cDNA was prepared with Multiscribe reverse transcriptase enzyme (High-Capacity cDNA Archive Kit; Applied Biosystems, Foster City, CA), and mRNA expression was measured in a RT-PCR reaction using TaqMan® gene expression assays and TaqMan® Universal PCR Master Mix No Amp Erase® (Applied Biosystems) on an ABI 7500 Fast Real-Time PCR System (Applied Biosystems). Threshold cycles (CT) were determined by an in-program algorithm assigning a fluorescence baseline based on readings prior to exponential amplification. An embryo RNA standard was used as a positive control. Fold change in expression was calculated using the $2^{-\Delta\Delta CT}$ method using 18 S RNA as an endogenous control [7].

2.5. Quantification of intracellular superoxide and LPA by mass spectrometry

Dihydroethidium (DHE, Invitrogen), which exhibits blue fluorescence in the cytosol until oxidized, was used to estimate the levels of superoxide after LPA treatment. The procedures for DHE were conducted using a FACScan protocol using a flow cytometry. For the quantitation of LPA molecular species, we used HPLC-tandem mass spectrometry as previously described [6,7]. Analysis of LPA was carried out using Waters Acquity UPLC coupled with a XEVO TQ-MS ESI mass

spectrometer. Sphingosine-1-phosphate (S1P) was used as an internal standard. S1P and LPA (Avanti Polar Lipid, Inc.) were separated using a Waters BEH C18 column, 1.7 µm, 2.1 × 50 mm column. The mobile phase consisted of 60/40 acetonitrile/water with formic acid (0.1%) and 5 mM ammonium formate (0.1%) as solvent A and 95/5 acetonitrile/water with formic acid (0.1%) and 5 mM ammonium formate (0.1%) as solvent B. For the analysis of S1P and LPA the separation was achieved using gradient of 0–100% B in the next 4 min, maintained at 100% B for the next 6 min and equilibrated back to the initial conditions in 5 min. The flow rate was 0.3 ml/min with a column temperature of 40 °C. The sample injection volume was 5 µL. The mass spectrometer was operated in full scan mode, scanning from *m/z* 70–500 with a scan time of 200 ms. The positive electrospray ionization mode for S1P and negative electrospray ionization mode for LPA were selected. The optimal ion source conditions were determined by S1P and LPA with a capillary voltage 3.82 V, cone voltage 17 V, desolvation temperature 450 °C, desolvation gas flow 1000 L/h, source temperature 150 °C, collision energy 10 V and Ion source temperature was 150 °C. S1P was detected by positive mode [M] + 365.2 and LPA was detected by negative mode [M-H] − 421.2 of full scan mode.

2.6. Mitochondrial isolation

Heart mitochondria were isolated as described previously by Mela and Seitz [16]. Briefly, the hearts were collected, washed in ice-cold isolation buffer (0.225 M mannitol, 0.075 M sucrose, 1 mM EGTA, pH 7.4), and was homogenized at 500 rpm with a chilled Teflon pestle in a glass cylinder with 10 strokes. The homogenate was centrifuged at 480 × *g* at 4 °C for 5 min. The pellet was rinsed with 0.5 ml of the isolation buffer with gentle shaking to remove the "fluffy layer" (damaged mitochondria) on top of the pellet. The wall of the centrifuge tube was cleaned with cotton swabs to remove lipids. The pellet was washed by

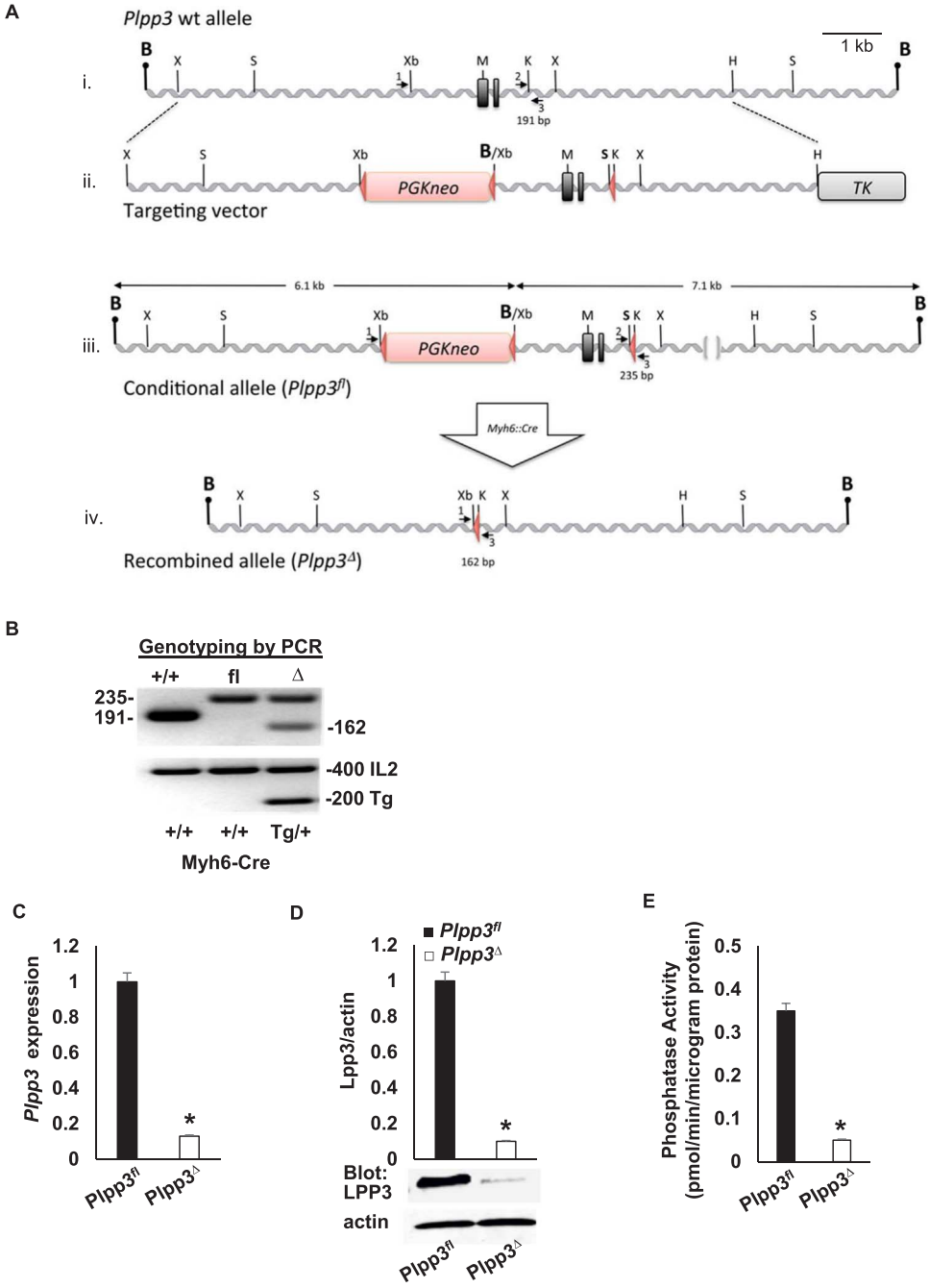

Fig. 1. Experimental design of the generation of *Plpp3*$^{\Delta}$ mice. A) Strategy for generating cardiac-specific alpha myosin-heavy chain LPP3 knockout mice. i) The genomic structure of an 11 kb *BamHI* fragment containing exons 3 and 4 of the wildtype *Plpp3* locus (gray boxes) and structure of the targeting construct. ii) A *floxed PGKneo* cassette was introduced upstream of exon 3, and an orphan *loxP* site and a *SalI* restriction site were introduced downstream of exon 4. iii) The structure of the targeted allele before (*Plpp3*^{fl}) and iv) after complete Cre-mediated recombination (*Plpp3*$^{\Delta}$). Small arrows with numbers show the position of oligonucleotides used for PCR genotyping and the size of the amplified products: X, *XmaI*; S, *SalI*; B, *BamHI*; Xb, *XbaI*; M, *MunI*; K, *KpnI*, H, *HindIII*; E, *EcoRI*. B) PCR screening for the totally recombined allele, orphan *loxP* present is 235 bp (fl), and excision of *PGKneo* and exons 3–4 is 162 bp (Δ). C) LPP3 mRNA expression was measured in heart tissue from *Plpp3*^{fl} and *Plpp3*$^{\Delta}$ mice and reported relative to values in *Plpp3*^{fl} heart (mean ± SD from n = 3 animals per genotype). D) Western blotting demonstrates LPP3 protein expression in *Plpp3*^{fl} and *Plpp3*$^{\Delta}$ with β-actin used as a loading control. LPP3 expression was normalized to β-actin staining (n = 3 animals) and presented as mean ± SD in arbitrary units in which the density of Lpp3 in the *Plpp3*^{fl} samples was set to 1. E) Lpp3 activity was determined in Lpp3 immunoprecipitates from the heart (n = 3 animals per genotype). Results are reported as pmol/min/µg protein (mean ± SD; n = 3 mice per genotype). *P < 0.05 by *t*-test vs control.

gentle resuspension in 3 ml isolation buffer using the smooth surface of a glass rod and centrifuged at 7700 × *g* at 4 °C for 10 min. At every step, the supernatant was saved to check again for leakage from the mitochondria. The resulting mitochondria were collected for further analysis. The purity of mitochondria was examined using Lamin B (a nuclear protein) and IκB-α (a cytoskeletal protein) as indicators by western blotting. Protein content in the lysate was determined by BCA protein assay (Pierce, Rockford, IL).

2.7. Mitochondrial bioenergetics

Oxygen consumption was determined using the Seahorse

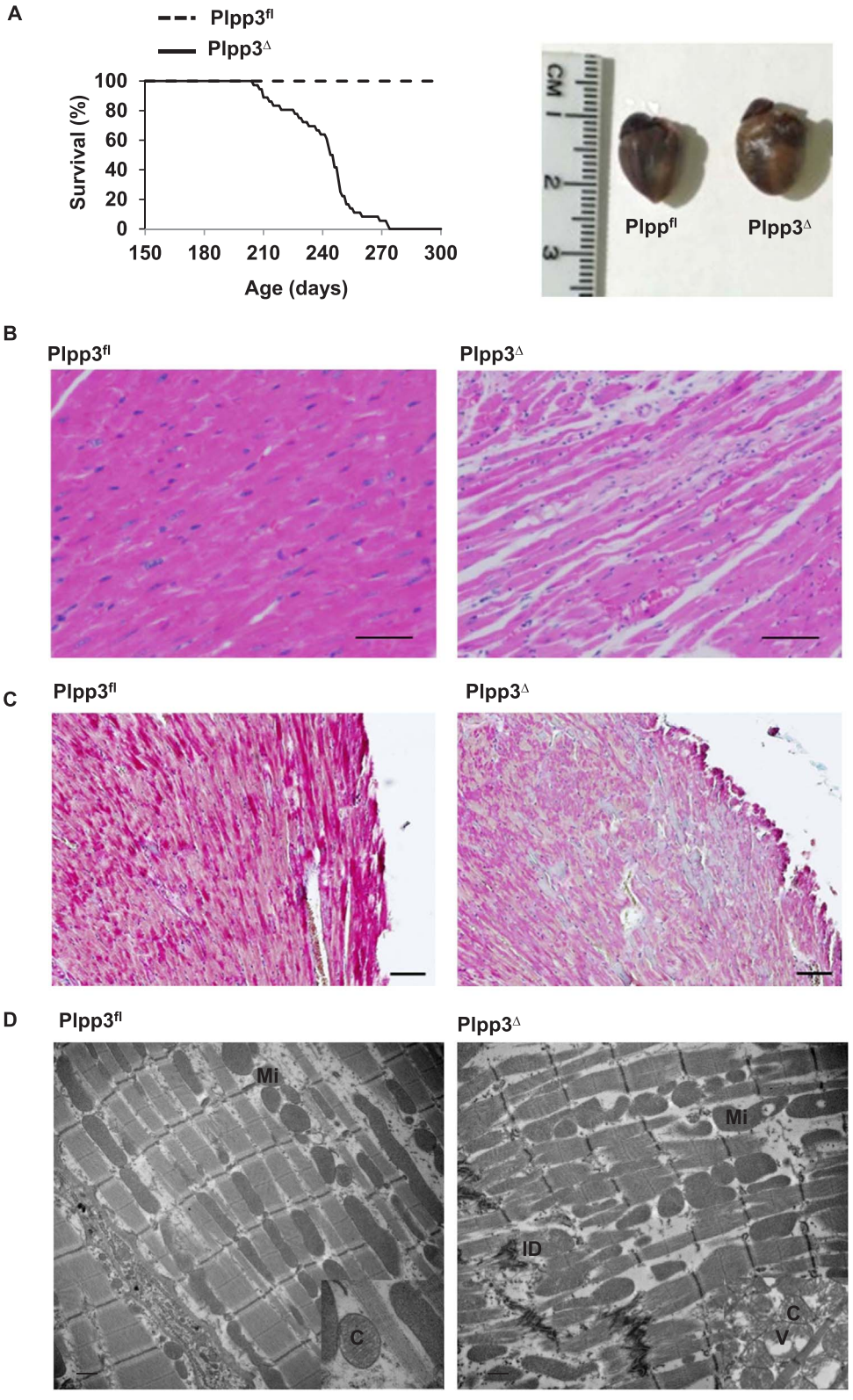

Fig. 2. Cardiac dysfunction exhibited in *Plpp3*$^{\Delta}$ mice. A) Kaplan-Meier analysis of survival probabilities for the *Plpp3*$^{\Delta}$ (n = 36) vs the *Plpp3*^{fl} (n = 38) animals (left) and the hearts of the 8-month-old *Plpp3*$^{\Delta}$ mice are significantly larger than the heart of the *Plpp3*^{fl} mice (right). B) Representative hematoxylin and eosin-stained hearts (LV) from *Plpp3*$^{\Delta}$ as compared to their *Plpp3*^{fl} littermates with immersion fixation. C) Masson's trichrome stained *Plpp3*$^{\Delta}$ hearts (LV) show increased density of connective tissue collagen matrix deposition. All analyses were carried out with 8-month-old mice. Scale bars 100 μm. D) Transmission electron micrograph of the 8-month-old myocardium (LV) from *Plpp3*$^{\Delta}$ as compared to their *Plpp3*^{fl} littermates. *Plpp3*$^{\Delta}$ myocardium showed distorted (ID) intercalated disc with damaged mitochondria (Mi). Mitochondrial insert showing disorganization of cristae (C), vacuole formation (V) and amorphous matrix densities in *Plpp3*$^{\Delta}$ as compared to *Plpp3*^{fl}. Bar denotes 500 nm.

Extracellular Flux (XF-24) analyzer (Seahorse Bioscience, Chicopee, MA). The XF-24 measures the concentration of oxygen and free protons in the medium above a monolayer of cells in real-time. Thus, the rates of oxygen consumption and proton production can be measured across several samples at a time. To allow comparison between experiments, data are presented as oxygen consumption rate (OCR) in pmol/min/μg

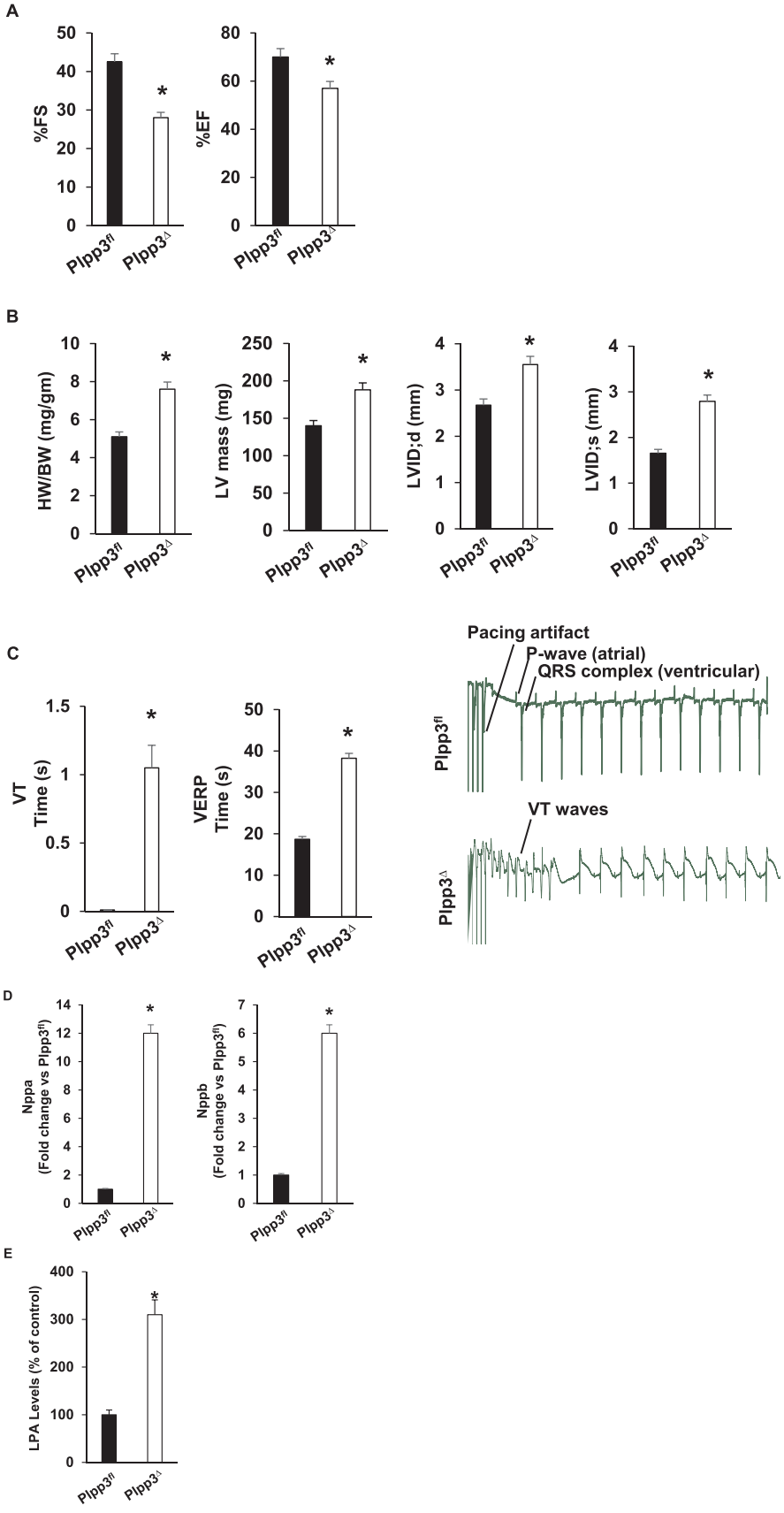

Fig. 3. Echocardiographic indices of *Plpp3*$^{\Delta}$ mice. A) Bar graph shows percentage changes in fractional shortening (%FS) and ejection fraction (%EF) in *Plpp3*$^{\Delta}$ mice compared to their *Plpp3*^{fl} littermates (n = 6) as measured echocardiography. B) Bar graph show representative hearts with an HW/BW ratio, left ventricular (LV) mass, diastolic left ventricular internal diameter (LVID; d) and systolic left ventricular internal diameter (LVID;s). C) Electrophysiology studies show inducible ventricular tachycardia (VT) and ventricular effective refractory periods (VERP) were significantly elevated in *Plpp3*$^{\Delta}$ mice as compared to their *Plpp3*^{fl} littermates (n = 6). D) Real-time RT-PCR shows fold differences in mRNA of *Nppa* and *Nppb* with the value of *Plpp3*^{fl} defined as 1 (mean ± SD, n = 4 each). *P < 0.05 by *t*-test vs control. E) Steady state plasma levels of total LPA from the circulation of live mice from *Plpp3*^{fl} control and *Plpp3*$^{\Delta}$ were measured by LC-MS/MS. Values are expressed as a fold increase over control and graphed as mean ± SD from n = 5 animals per time point. *P < 0.01 compared to control.

protein and the extracellular acidification rate (ECAR) in mpH/min/μg protein. Neonatal cardiomyocytes were seeded at 100,000 cells/well into gelatin-coated Seahorse Bioscience XF microplates, cultured in the presence or absence of 2 g/L D-glucose, and then centrifuged to adhere to the bottom of the wells. OCR was measured four times and plotted as a function of cells under the basal condition followed by the sequential addition of oligomycin (1 μg/ml, an inhibitor of mitochondrial ATP-synthase) was injected into the XF medium to estimate the OCR coupled to ATP synthesis and represented as ATP-linked. The residual oligomycin/OCR minus the non-mitochondrial OCR (after antimycin A treatment) can be attributed to proton leak. FCCP (0.5 μM), an uncoupler, is added to determine the maximal OCR, followed by antimycin (1 μM), an inhibitor of mitochondrial respiration, to determine non-mitochondrial sources of oxygen consumption. The ATP-linked OCR was calculated as the difference between the basal OCR and the OCR measured after the addition of oligomycin. The OCR maximal capacity was the direct rate measured after the addition of FCCP minus non-mitochondrial respiration. Spare respiratory capacity is a measure of the amount of ATP that can be produced under energetic demand and can be calculated as the difference between the maximum rate of respiration and the basal. The OCR values were normalized to total protein content in the corresponding wells and expressed as pmol/min/mg protein.

To calculate ECAR measurements, cells were washed and changed to assay medium lacking glucose. Basal ECAR were measured four times and plotted as a function of cells under the basal condition followed by the sequential addition of glucose (25 mM), oligomycin (1 μg/ml) and 2-deoxyglucose (25 mM), an inhibitor for the hexokinase. The rate of glycolysis was determined by the difference between the basal ECAR from the ECAR after the addition of glucose. The glycolytic reserve was determined by subtracting the ECAR following the addition of oligomycin from the ECAR following the addition of glucose.

2.8. Histology and electron microscopy

The hearts were collected at 8 months of age, fixed in 10% buffered formalin, and embedded in paraffin. Serial 5-μm heart sections from each group were stained with hematoxylin and eosin or Masson's trichrome [17]. For electron microscopy, the left ventricles were dissected from hearts, and fixed in 2% EM-grade glutaraldehyde (Sigma), 2% PFA in 0.2 M sodium cacodylate (pH 7.4; Sigma) overnight at 4 °C, and post-fixed in 1% osmium tetroxide (EM Sciences) in 0.2 M sodium cacodylate (pH 7.4) for 2 h at 4 °C. Tissue was treated with propylene oxide and resin embedded (EMBED 812 kit, EM Sciences). The osmicated samples were then dehydrated through a series of graded ethanol solutions and then infiltrated with propylene oxide (EM Sciences). Subsequently, the tissues were infiltrated with Durcupan ANC Fluka Araldite (Sigma Chemical) and embedded in the same resin. After polymerization, 80-nm sections were cut using a Reichert Ultracut E Ultramicrotome (Leica Microsystems, Bannockburn, IL), and the grids were subsequently stained with uranyl acetate and lead citrate. The sections were imaged using a Hitachi transmission electron microscope equipped for digital image acquisition.

2.9. Statistical analysis

Unless otherwise stated, results were expressed as a mean ± standard deviation of the mean. In vitro studies were repeated a minimum of three times. One-way analysis of variance (ANOVA) followed by the Bonferroni post hoc test or the unpaired Student's *t*-test was used to identify significant differences between groups. Statistical analysis was performed using Sigma-STAT software, version 3.5 (Systat Software Inc., San Jose, CA, USA). A P-value of less than 0.05 was considered significant.

3. Results

3.1. Generation of mice deficient in LPP3 in cardiac myocytes

Global deletion of *Plpp3* results in embryonic lethality due to failure to develop an extraembryonic vasculature [5]. Furthermore, we have identified that even a tissue specific deficiency of endothelial-LPP3 exhibits embryonic lethality due to defective cardiovascular development [6] and inducible knockouts of LPP3 show enhanced inflammation and permeability [6,7]. To study the biological function of LPP3 in the heart, we generated cardiomyocyte specific *Plpp3* knockout mice. For this purpose, we utilized $Plpp3^{fl}$ mice with two *loxP* sites flanking exons 3 and 4 of the *Plpp3* locus [18]. These mice were crossed with mice expressing Cre recombinase under the control of the cardiac-specific alpha-myosin heavy chain promoter (*Myh6-Cre*) [12] to generate Myh6-LPP3-deficient mice ($Plpp3^{\Delta}$) (Fig. 1A).

3.2. Analysis of LPP3 expression

Recombination in the *Plpp3* locus was confirmed by PCR analysis (Fig. 1B). To provide biochemical evidence that LPP3 expression is deficient in the heart, we looked at mRNA expression of LPP3 in knockout mice heart tissue, which was confirmed to be negligible when compared to the $Plpp3^{fl}$ mice (Fig. 1C). Immunoblot analysis of heart tissue was performed to determine LPP3 protein expression. As shown in Fig. 1D, LPP3 expression was negligible in the heart from $Plpp3^{\Delta}$ mice, when compared to $Plpp3^{fl}$ hearts. When we compare the contribution of LPP3 in cardiomyocytes over the other two isoforms of phospholipid phosphatases, namely, LPP1 and LPP2, the significantly reduced phosphatase activity in our $Plpp3^{\Delta}$ mice suggest that LPP3 has a more prominent role in the heart (Fig. 1E).

3.3. Mice lacking LPP3 in the heart have shorter life spans due to decreased cardiac function

Unlike global *Plpp3* knockout mice, $Plpp3^{\Delta}$ are viable and fertile. All mice reached adulthood with no obvious phenotype. However, they had a decreased life span of ~ 8 months (Fig. 2A). 3-month-old $Plpp3^{\Delta}$ mice showed higher heart rates (642 ± 21 bpm) compared to $Plpp3^{fl}$ mice (580 ± 17 bpm; $P < 0.01$) although the blood pressure was similar in mice from both genotypes (96 ± 9 mmHg; $n = 19$ in $Plpp3^{fl}$ as compared to 92 ± 7 mmHg; $n = 19$ in $Plpp3^{\Delta}$). After 7 months of age, mutant mice displayed signs of progressive heart failure. They had enlarged hearts indicating dilated cardiomyopathy (Fig. 2A). Cardiac tissue samples from 8-month-old mice were stained with hematoxylin and eosin staining (Fig. 2B) to compare the myocardium. $Plpp3^{\Delta}$ hearts exhibited sarcomere disarray whereas $Plpp3^{fl}$ hearts had no abnormalities. Masson's trichrome stained $Plpp3^{\Delta}$ hearts showed increased density of connective tissue collagen matrix deposition (Fig. 2C). Ultrastructural studies in $Plpp3^{\Delta}$ heart tissue demonstrated myofilament destruction and absence of glycogen with distinct disruption of the intercalated discs. Mitochondria showed vacuole formation with prominent disruption of the cristae and rupture of the double membrane with deposition of an amorphous dense body (Fig. 2D).

Based on the evidence described above, we sought to determine the performance of the left ventricle in 8-month-old knockout mice using echocardiography. We observed a significant reduction in the fractional shortening as well as ejection fraction in mice lacking LPP3 in the heart, suggesting a decline in the left ventricular function (Fig. 3A). The heart weight/body weight (HW/BW) ratio and left ventricular (LV) mass index were also significantly elevated in $Plpp3^{\Delta}$ compared to $Plpp3^{fl}$ control mice (Fig. 3B). $Plpp3^{\Delta}$ mice had longer ventricular effective refractory periods compared to their $Plpp3^{fl}$ littermates (38.25 ± 1.181 vs 18.67 ± 0.6667). These mice also had a higher incidence of inducible VT with 1.050 ± 0.1652 s of VT compared to the controls (Fig. 3C). Natriuretic peptide A and B (*Nppa* and *Nppb*) are secreted by

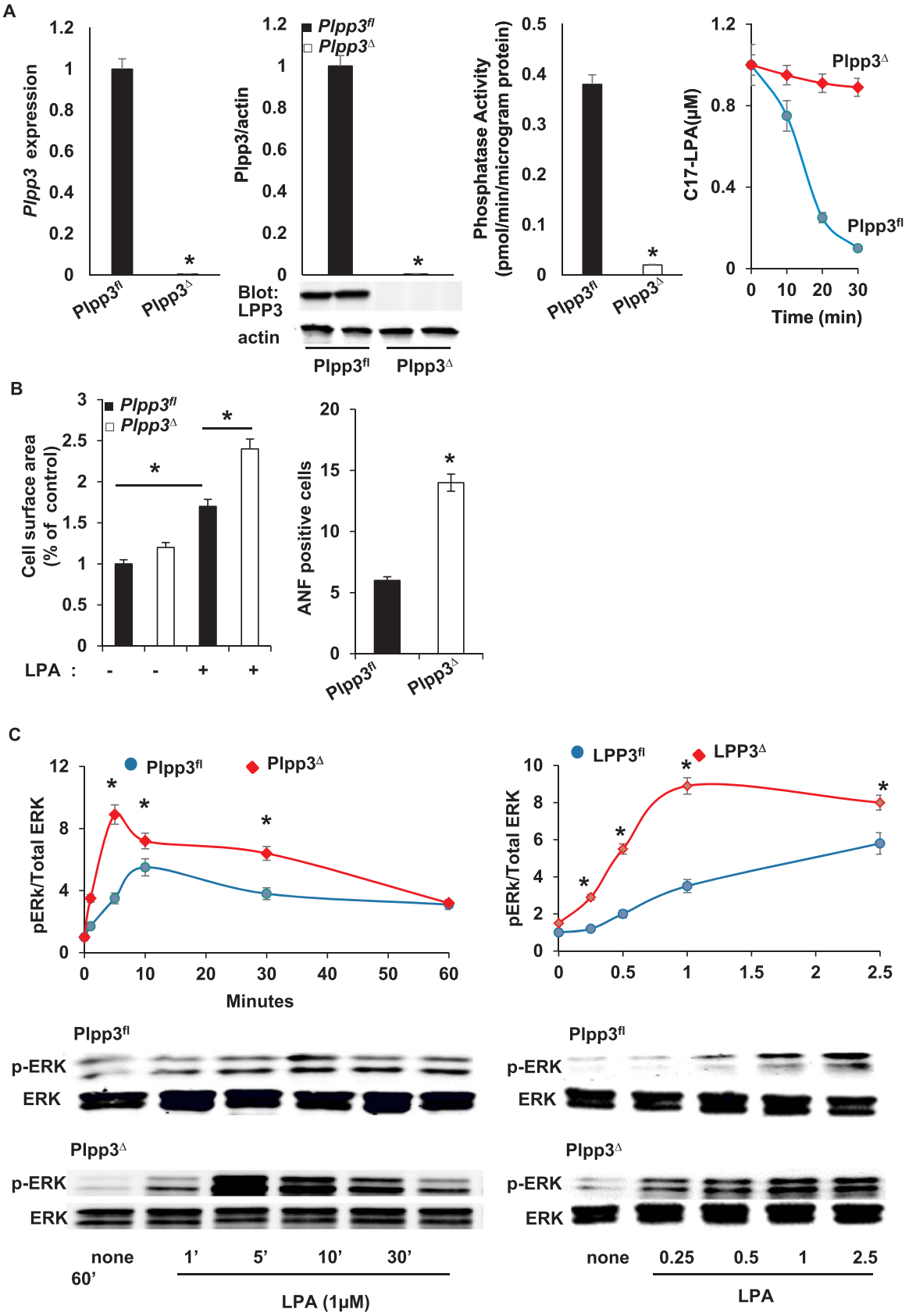

Fig. 4. LPP3 negatively regulates LPA signaling responses in neonatal cardiomyocytes. A) expression, immunoblot and activity assay showed the absence of LPP3 in *Plpp3*$^{\Delta}$ cardiomyocytes (n = 4). B) Increase cell surface area is observed upon stimulation with LPA (1 μM) in *Plpp3*$^{\Delta}$ cardiomyocytes with increased ANF positive cells (n = 4). B) and C) *Plpp3*$^{\Delta}$ cardiomyocytes showed increased levels of extracellular signal-regulated kinase (ERK) activation upon stimulation with LPA (1 μM) at different time point intervals (n = 3). Where indicated, cells were infected with lentivirus expressing human (h) LPP3 or a catalytically inactive LPP3 variant. D) *Plpp3*$^{\Delta}$ cardiomyocytes showed increased levels of Rho activation upon stimulation with LPA (1 μM) (n = 3). E) ERK activation was measured in *Plpp3*^{fl} and *Plpp3*$^{\Delta}$ cardiomyocytes 5 min after treatment with 2.5 μmol/L of the nonhydrolyzable LPA analog 1-oleoyl-2-O-methyl-rac-glycerophosphothionate (OMPT) (n = 3). *P < 0.01 by 1-way ANOVA.

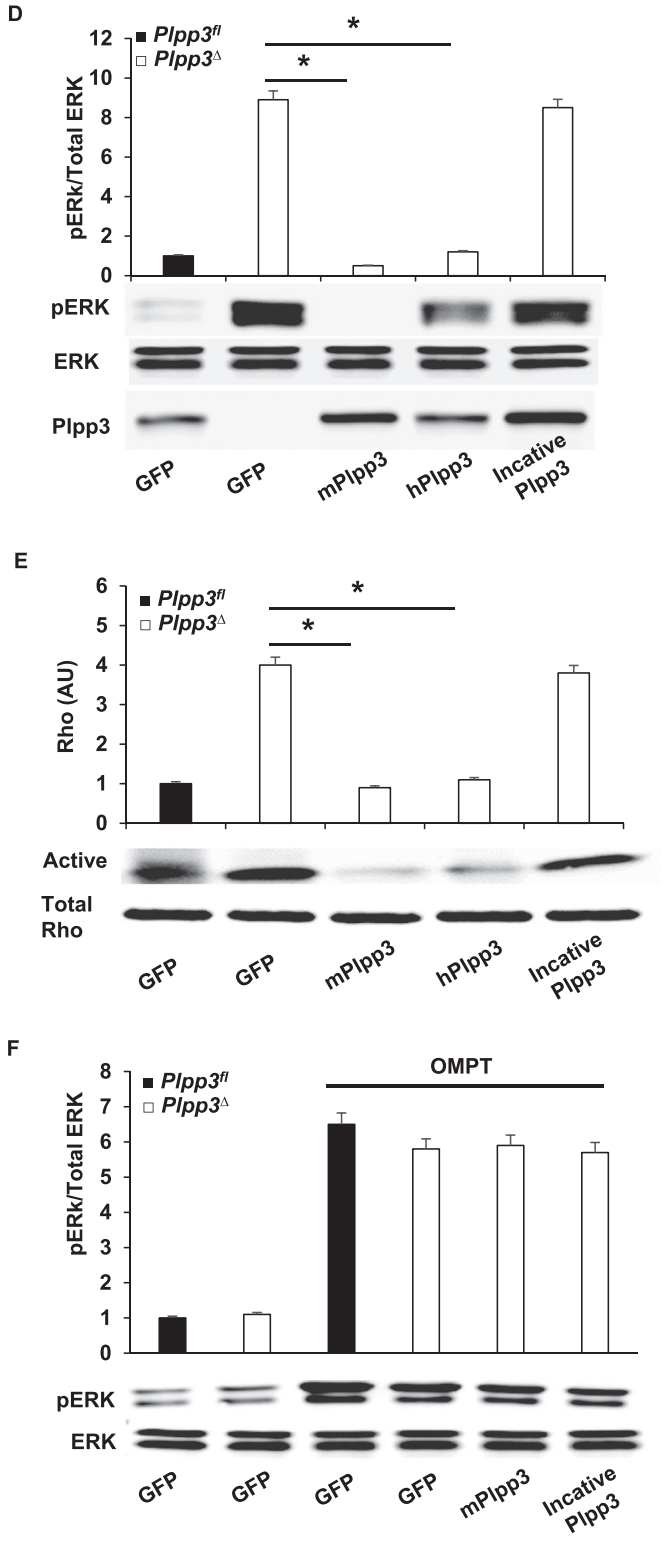

Fig. 4. (*continued*)

the heart in response to cardiomyopathy, so we measured their levels in the failing *Plpp3*$^{\Delta}$ hearts. As shown in Fig. 3D, an increase in the expression of these cardiomyocyte stress-response genes was observed. Together, these results suggest that LPP3 is essential for cardiac function. Since the role of LPP3 is dephosphorylation of LPA, we measured LPA levels in the plasma. The circulating plasma levels of LPA were increased ≈ 2-fold in the *Plpp3*$^{\Delta}$ mice as compared to *Plpp3*^{fl} littermates (Fig. 3E).

3.4. LPP3 negatively regulates LPA signaling responses in cardiomyocytes

Lipid phosphatase activity measured in LPP3 immunoprecipitates accounted for less than 5% phosphatase activity in *Plpp3*$^{\Delta}$ cardiomyocytes confirming that LPP3 is the predominant isoform in the myocardium (Fig. 4A). Furthermore, direct measurement of lipids in intact cells to determine LPA phosphatase activity showed that exogenously applied C17-LPA was degraded 6-fold more slowly by *Plpp3*$^{\Delta}$ than control cells (Fig. 4A). Treatment with LPA led to a significantly higher increase in cell surface area in the *Plpp3*$^{\Delta}$ cardiomyocytes. The number of ANF (Atrial Natriuretic Factor) positive cells, a biomarker of cardiovascular disease, was also higher in *Plpp3*$^{\Delta}$ cardiomyocytes (Fig. 4B). The lack of LPP3 in cardiomyocytes enhanced LPA-mediated phospho-ERK activation by increasing and prolonging ERK phosphorylation. In comparison to *Plpp3*^{fl} cardiomyocytes, *Plpp3*$^{\Delta}$ cardiomyocytes demonstrated a robust increase in LPA-induced phospho-ERK activation that persisted for up to 30 min ($P < 0.001$; Fig. 4C). Additionally, *Plpp3*$^{\Delta}$ cardiomyocytes responded to lower levels of LPA, with an ≈ 3-fold increase in ERK activation at 5 min in response to 1 μM LPA ($P < 0.001$; Fig. 4C). Expression of murine or human LPP3, but not a catalytically inactive LPP3 mutant, rescued the phenotype of *Plpp3*$^{\Delta}$ cardiomyocytes by reducing phosphorylation of ERK in response to LPA (Fig. 4D). Rho activation in response to LPA was also enhanced in *Plpp3*$^{\Delta}$ cardiomyocytes ($P < 0.001$) and was corrected by overexpression of either murine or human LPP3, but not a catalytically inactive mutant (Fig. 4E). If LPP3-deficient cells showed enhanced LPA-signaling due to a reduction in LPA degradation, then the *Plpp3*$^{\Delta}$ cardiomyocytes should respond normally to a poorly hydrolyzable receptor-active LPA mimetic, such as the ester-linked thiophosphate derivative (1-oleoyl-2-O-methyl-rac-glycerophosphothionate, OMPT). To emphasize the need for enzymatic catalytic function, we found that OMPT-stimulated ERK activation responses of *Plpp3*^{fl} and *Plpp3*$^{\Delta}$ cardiomyocytes were similar (Fig. 4F).

3.5. LPP3 is required for cardiomyocyte mitochondrial respiration and function

Since the mitochondrial damage was observed, as shown in Fig. 2, we isolated mitochondria from the myocardium of the 8-month-old *Plpp3*$^{\Delta}$ mice. These were used to determine the impact of LPP3 on mitochondrial bioenergetics. Mitochondria from *Plpp3*$^{\Delta}$ hearts showed a significant decrease ($P < 0.001$; Fig. 5A and B) in the basal oxygen consumption rate, mitochondrial ATP production, maximal respiration and spare respiratory capacity when compared to the same parameters found in mitochondria from *Plpp3*^{fl} hearts. To further clarify the role of LPP3 in the myocardium, we used neonatal cardiomyocytes to determine the mitochondrial activity and superoxide levels. There also was a significant reduction in the basal oxygen consumption rate, mitochondrial ATP production, maximal respiration and spare respiratory capacity of neonatal *Plpp3*$^{\Delta}$ cardiomyocytes ($P < 0.001$; Fig. 5C and D). We examined glycolysis in these neonatal cardiomyocytes by ECAR, and the opposite pattern to OCR was observed for glycolysis rates between *Plpp3*$^{\Delta}$ and *Plpp3*^{fl} cardiomyocytes (Fig. 5E). The reverse relation of oxidative phosphorylation and glycolysis rates indicated changes in the metabolism for energy generation in *Plpp3*$^{\Delta}$ and *Plpp3*^{fl} cardiomyocytes and is indicative of an early mitochondrial dysfunction in *Plpp3*$^{\Delta}$ hearts. Then, we determined the free radical regulation of *Plpp3*$^{\Delta}$ cardiomyocytes by measuring the superoxide anion using a fluorescent cholesterol analog, dihydroethidium. Increased basal superoxide production was observed in neonatal *Plpp3*$^{\Delta}$ cardiomyocytes. When treated with LPA, *Plpp3*$^{\Delta}$ cardiomyocytes showed higher superoxide levels as compared to LPA-treated *Plpp3*^{fl} cells. LPA-induced superoxide production was lowered by the addition of mitoTEMPO, a mitochondrial-specific superoxide scavenger. A similar reduction of superoxide was observed by the reintroduction of LPP3 expression (Fig. 5F). These findings point to the significance of LPP3 expression in mitochondrial

oxidative phosphorylation as well as in the normal physiology of the myocardium in adult mice.

4. Discussion

LPP3 is a regulator of cell signaling because of its role in the dephosphorylation of LPA, which has been implicated in the many cardiovascular diseases [10,11,8]. To provide insight into the role of LPP3 in the cardiovascular system, we developed the heart specific *Plpp3* knockout mice. The data obtained in *Plpp3*$^{\Delta}$ mice indicate that although lack of LPP3 in the cardiomyocytes allows for the normal development of the heart, it is critical for optimal functioning in adult mice. Several independent genome-wide association studies revealed a link between a frequently occurring polymorphism in the *Plpp3 locus* with an increased risk of coronary artery disease [19–21]. Our previous studies demonstrated that lack of LPP3 in endothelial and a subset of hematopoietic cells resulted in embryonic lethality with striking cardiovascular development defects [6]. Although the effects of LPP3 have been widely studied, little is known about LPA-mediated signaling pathways that are regulated by LPP3 in the myocardium.

In the current study, we have demonstrated that the absence of LPP3 in cardiomyocytes leads to progressive heart failure and a significantly shortened life span in mice (Fig. 3). Cardiac specific deletion of *Plpp3* results in mice which survive and are fertile but more interestingly, their cardiac function and structure are normal at younger age, suggesting that either LPP3 expressed in the cardiomyocytes does not play an essential role in early cardiovascular development or the alpha myosin heavy chain – Cre/*loxP* system used in the generation of these mice allows LPP3 expression in the cardiomyocytes during early embryogenesis.

These mice have normal cardiac function and histology up to 3 months of age. Although these mice seem to have no cardiac functional abnormalities at a young age, it is possible that use of more invasive measurements along with increased cardiac workload may uncover underlying conditions. After 7 months of age, the lack of LPP3 in *Plpp3*$^{\Delta}$ mice resulted in a two-fold increase in the circulating LPA compared to its *Plpp3*^{fl} counterparts. Left ventricular (LV) function, as measured by the percent of fractional shortening (%FS) and ejection fraction (%EF), was prominently decreased in *Plpp3*$^{\Delta}$ mice. Also, cardiomyocyte disarray and sarcomere disruption were evident in the failing hearts that lacked LPP3. Furthermore, transmission electron micrograph studies revealed fragmentation and disorientation of myofibrils, distinct disruption of the intercalated discs, intermyofibrillar edema, rupture of cristae and double membrane with deposition of amorphous dense bodies in the failing myocardium of the *Plpp3*$^{\Delta}$ mice.

The use of neonatal cardiomyocytes allowed us to show that LPP3 regulates LPA-mediated phosphorylation of ERK, Rho activation, cardiomyocyte hypertrophy and genetic markers of cardiac stress such as atrial natriuretic factor (Nppa) and B-type natriuretic peptide (Nppb). Although LPP1 and LPP2 have the same catalytic function as that of LPP3, gene inactivation of *Plpp1* or *Plpp2* has been reported to produce no phenotypic alteration in the myocardium [5,22,23]. Furthermore, direct measurements of intact cell LPA phosphatase activity in our *Plpp3*$^{\Delta}$ cardiomyocytes demonstrated that LPP3 is the major isoform that regulates the LPA-mediated signaling in the myocardium. Since LPP3 also regulates the dephosphorylation of PA, which is known to induce cardiac hypertrophy [24], further studies are needed to determine the effect of cardiomyocyte specific LPP3 knockout on other phospholipids in the myocardium.

The fatty acid is considered to be the major metabolic substrate for the normal adult heart at resting stage. Glucose and lactate account for about 25–30% of myocardial ATP production. Although glucose is not the predominant fuel for the adult heart at resting stage as compared to that of the neonatal cardiomyocytes, the heart switches substrate preference from fatty acid to glucose at many circumstances during stress such as ischemia and pathological hypertrophy [25]. Studies have shown simple glycerophospholipid LPA-mediated ROS production in cell culture models [26,27], however, its effect on mitochondrial bioenergetics in cardiomyocytes needs more research. Our real-time observation studies on mitochondrial oxidative phosphorylation status revealed mitochondrial dysfunction with increased production of superoxide (a normal byproduct of oxidative phosphorylation that is formed at increased rates when the electron transport chain is defective) in the cardiomyocytes that lack LPP3. Oxidative stress was mitigated by the re-expression of LPP3. These findings indicate an important role for LPP3 in the prevention of oxidative stress caused by mitochondrial dysfunction. Our data add to the weight of the evidence that LPP3 regulates cardiomyocyte function. Although the lack of LPP3 clearly impairs LPA degradation and inactivation, additional non–LPA-dependent mechanisms of LPP3 action could also affect cardiomyocyte function. For example, LPP3 have non-enzymatic functions mediated by integrin binding or β-catenin signaling [5,28].

Emerging evidence supports a role for lysophospholipid mediators in the regulation of cardiac development and function [6,7,28]. Our findings provide functional evidence for a novel role of LPP3 mediated lipid metabolism in adult myocardium. Longer VERPs observed in *Plpp3*$^{\Delta}$ mice could mean that the action potentials are longer in these animals, which could then cause early and delayed afterdepolarizations leading to arrhythmias [29,30]. Infusion of LPA in rabbits increases ventricular arrhythmia and the proportion of non-phosphorylated connexin43, which may inhibit junction transmission [31]. Whether LPP3 regulates any of these responses is not known. Future studies should address these intriguing questions.

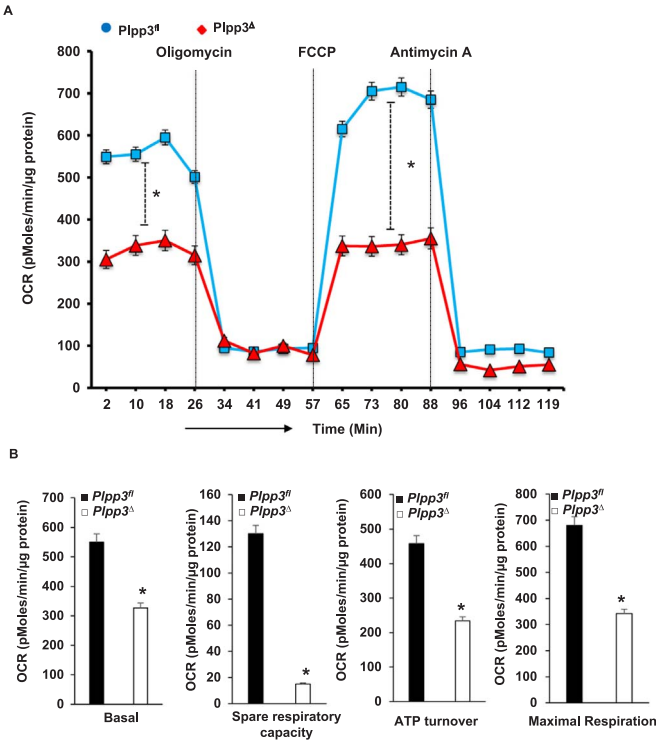

Fig. 5. Mitochondrial activities in *Plpp3*$^{\Delta}$ mitochondria (A and B) and neonatal cardiomyocytes. (C and D). Oxygen consumption rate (OCR, pmol/min/µg protein) determined with XF24 analyzer oxidative phosphorylation activity. Extracellular acidification rate (ECAR) by XF24 analyzer for glycolysis activity (E). Superoxide radicals produced in the cardiomyocytes were analyzed using a dihydroethidium fluorescence probe (F). All values are mean ± SD (n = 5). *P < 0.05 as compared to control; #P < 0.05 as compared to LPA (1 µM) stimulated cells.

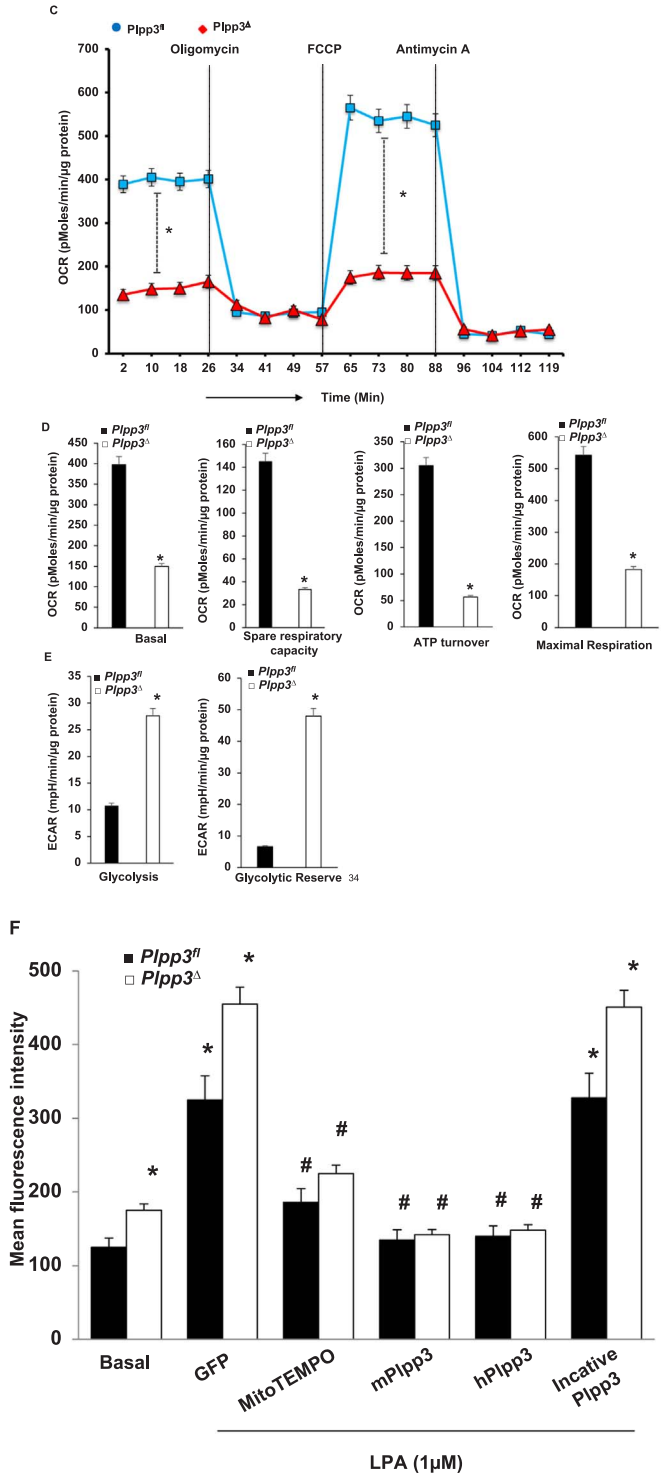

Fig. 5. (*continued*)

5. Conclusions

The results presented in this study indicate that the loss of LPP3 in cardiomyocytes impairs the myocardial function. Importantly, we demonstrate that LPP3 is a modifier of LPA-mediated signaling in the myocardium. Taken together, this study is crucial for the understanding of the importance of LPP3 in the preservation of cardiac structure and function. In addition, this model also provides an important tool for furthering our knowledge in the understanding of LPA signaling in cardiomyocytes pertaining to various heart diseases.

Acknowledgements

The authors thank the Center for Cardiovascular Disease and Sciences (CCDS) imaging and mass spectrometry Core for echocardiography and lipid estimation and the Animal Care Committee and the Veterinary staffs at the Louisiana State University Health Sciences Center, Shreveport, for their help with animal experiments at the vivarium. Joe Jones, Megan Watts, and Ronald Maloney provided excellent technical support.

Conflict of interest

None declared.

Funding

This work was supported by American Heart Association Scientist Development Grant 10SDG4190036 to Dr. Panchatcharam; Louisiana State University Health Sciences – Shreveport Intramural Grant 110101074A to Dr. Miriyala; National Institutes of Health Grants HL098435 and HL133497 to Dr. Orr and R00 HL122354 to Dr. Bhuiyan. Funding to pay the publication charges for this article was provided by Dr. Panchatcharam.

References

[1] H. Ren, M. Panchatcharam, P. Mueller, D. Escalante-Alcalde, A. Morris, S. Smyth, Lipid phosphate phosphatase (LPP3) and vascular development, Biochim. Biophys. Acta 1831 (1) (2013) 126–132.
[2] F. Alderton, P. Darroch, B. Sambi, A. McKie, I.S. Ahmed, N. Pyne, S. Pyne, G-protein-coupled receptor stimulation of the p42/p44 mitogen-activated protein kinase pathway is attenuated by lipid phosphate phosphatases 1, 1a, and 2 in human embryonic kidney 293 cells, J. Biol. Chem. 276 (16) (2001) 13452–13460.
[3] V.A. Sciorra, A.J. Morris, Sequential actions of phospholipase D and phosphatidic acid phosphohydrolase 2b generate diglyceride in mammalian cells, Mol. Biol. Cell 10 (11) (1999) 3863–3876.
[4] E. Gutierrez-Martinez, I. Fernandez-Ulibarri, F. Lazaro-Dieguez, L. Johannes, S. Pyne, E. Sarri, G. Egea, Lipid phosphate phosphatase 3 participates in transport carrier formation and protein trafficking in the early secretory pathway, J. Cell Sci. 126 (Pt 12) (2013) 2641–2655.
[5] D. Escalante-Alcalde, L. Hernandez, H. Le Stunff, R. Maeda, H.S. Lee, C. Gang Jr, V.A. Sciorra, I. Daar, S. Spiegel, A.J. Morris, C.L. Stewart, The lipid phosphatase LPP3 regulates extra-embryonic vasculogenesis and axis patterning, Development 130 (19) (2003) 4623–4637.
[6] M. Panchatcharam, A.K. Salous, J. Brandon, S. Miriyala, J. Wheeler, P. Patil, M. Sunkara, A.J. Morris, D. Escalante-Alcalde, S.S. Smyth, Mice with targeted inactivation of ppap2b in endothelial and hematopoietic cells display enhanced vascular inflammation and permeability, Arterioscler. Thromb. Vasc. Biol. 34 (4) (2014) 837–845.
[7] A.K. Salous, M. Panchatcharam, M. Sunkara, P. Mueller, A. Dong, Y. Wang, G.A. Graf, S.S. Smyth, A.J. Morris, Mechanism of rapid elimination of lysophosphatidic acid and related lipids from the circulation of mice, J. Lipid Res. 54 (10) (2013) 2775–2784.
[8] X. Chen, X.Y. Yang, N.D. Wang, C. Ding, Y.J. Yang, Z.J. You, Q. Su, J.H. Chen, Serum lysophosphatidic acid concentrations measured by dot immunogold filtration assay in patients with acute myocardial infarction, Scand. J. Clin. Lab. Investig. 63 (7–8) (2003) 497–504.
[9] M. Panchatcharam, S. Miriyala, F. Yang, M. Rojas, C. End, C. Vallant, A. Dong, K. Lynch, J. Chun, A.J. Morris, S.S. Smyth, Lysophosphatidic acid receptors 1 and 2 play roles in regulation of vascular injury responses but not blood pressure, Circ. Res. 103 (6) (2008) 662–670.
[10] J. Chen, Y. Chen, W. Zhu, Y. Han, B. Han, R. Xu, L. Deng, Y. Cai, X. Cong, Y. Yang, S. Hu, X. Chen, Specific LPA receptor subtype mediation of LPA-induced hypertrophy of cardiac myocytes and involvement of Akt and NFκB signal pathways, J. Cell. Biochem. 103 (6) (2008) 1718–1731.
[11] J. Yang, Y. Nie, F. Wang, J. Hou, X. Cong, S. Hu, X. Chen, Reciprocal regulation of miR-23a and lysophosphatidic acid receptor signaling in cardiomyocyte hypertrophy, Biochim. Biophys. Acta (BBA) – Mol. Cell Biol. Lipids 1831 (8) (2013) 1386–1394.
[12] R. Agah, P.A. Frenkel, B.A. French, L.H. Michael, P.A. Overbeek, M.D. Schneider, Gene recombination in postmitotic cells. Targeted expression of Cre recombinase provokes cardiac-restricted, site-specific rearrangement in adult ventricular muscle in vivo, J. Clin. Investig. 100 (1) (1997) 169–179.
[13] E. Ehler, T. Moore-Morris, S. Lange, Isolation and culture of neonatal mouse cardiomyocytes, J. Vis. Exp. 79 (2013).
[14] M.S. Bhuiyan, P. McLendon, J. James, H. Osinska, J. Gulick, B. Bhandary, J.N. Lorenz, J. Robbins, In vivo definition of cardiac myosin-binding protein C's critical interactions with myosin, Pflug. Arch. 468 (10) (2016) 1685–1695.

[15] C.T. Maguire, H. Wakimoto, V.V. Patel, P.E. Hammer, K. Gauvreau, C.I. Berul, Implications of ventricular arrhythmia vulnerability during murine electrophysiology studies, Physiol. Genom. 15 (1) (2003) 84–91.
[16] L. Mela, S. Seitz, Isolation of mitochondria with emphasis on heart mitochondria from small amounts of tissue, Methods Enzymol. (1979) 39–46 ([4]).
[17] S. Bhuiyan, P. McLendon, J. James, H. Osinska, J. Gulick, B. Bhandary, J.N. Lorenz, J. Robbins, In vivo definition of cardiac myosin-binding protein C's critical interactions with myosin, Pflug. Arch.: Eur. J. Physiol. 468 (10) (2016) 1685–1695.
[18] D. Escalante-Alcalde, R. Sánchez-Sánchez, C.L. Stewart, Generation of a conditional Ppap2b/Lpp3 null allele, genesis 45 (7) (2007) 465–469.
[19] H. Schunkert, I.R. Konig, S. Kathiresan, M.P. Reilly, T.L. Assimes, H. Holm, M. Preuss, A.F. Stewart, M. Barbalic, C. Gieger, D. Absher, Z. Aherrahrou, H. Allayee, D. Altshuler, S.S. Anand, K. Andersen, J.L. Anderson, D. Ardissino, S.G. Ball, A.J. Balmforth, T.A. Barnes, D.M. Becker, L.C. Becker, K. Berger, J.C. Bis, S.M. Boekholdt, E. Boerwinkle, P.S. Braund, M.J. Brown, M.S. Burnett, I. Buysschaert, Cardiogenics, J.F. Carlquist, L. Chen, S. Cichon, V. Codd, R.W. Davies, G. Dedoussis, A. Dehghan, S. Demissie, J.M. Devaney, P. Diemert, R. Do, A. Doering, S. Eifert, N.E. Mokhtari, S.G. Ellis, R. Elosua, J.C. Engert, S.E. Epstein, U. de Faire, M. Fischer, S. Folsom, J. Freyer, B. Gigante, D. Girelli, S. Gretarsdottir, V. Gudnason, J.R. Gulcher, E. Halperin, N. Hammond, S.L. Hazen, A. Hofman, B.D. Horne, T. Illig, C. Iribarren, G.T. Jones, J.W. Jukema, M.A. Kaiser, L.M. Kaplan, J.J. Kastelein, K.T. Khaw, J.W. Knowles, G. Kolovou, A. Kong, R. Laaksonen, D. Lambrechts, K. Leander, G. Lettre, M. Li, W. Lieb, C. Loley, A.J. Lotery, P.M. Mannucci, S. Maouche, N. Martinelli, P.P. McKeown, C. Meisinger, T. Meitinger, O. Melander, P.A. Merlini, V. Mooser, T. Morgan, T.W. Muhleisen, J.B. Muhlestein, T. Munzel, K. Musunuru, V. Nahrstaedt, C.P. Nelson, M.M. Nothen, O. Olivieri, R.S. Patel, C.C. Patterson, A. Peters, F. Peyvandi, L. Qu, A.A. Quyyumi, D.J. Rader, L.S. Rallidis, C. Rice, F.R. Rosendaal, D. Rubin, V. Salomaa, M.L. Sampietro, M.S. Sandhu, E. Schadt, A. Schafer, A. Schillert, S. Schreiber, J. Schrezenmeir, S.M. Schwartz, D.S. Siscovick, M. Sivananthan, S. Sivapalaratnam, A. Smith, T.B. Smith, J.D. Snoep, S. Soranzo, J.A. Spertus, K. Stark, K. Stirrups, M. Stoll, W.H. Tang, S. Tennstedt, G. Kastelein, G. Thorleifsson, M. Tomaszewski, A.G. Uitterlinden, A.M. van Rij, B.F. Voight, N.J. Wareham, G.A. Wells, H.E. Wichmann, P.S. Wild, C. Willenborg, J.C. Witteman, B.J. Wright, S. Ye, T. Zeller, A. Ziegler, F. Cambien, A.H. Goodall, L.A. Cupples, T. Quertermous, W. Marz, C. Hengstenberg, S. Blankenberg, W.H. Ouwehand, A.S. Hall, P. Deloukas, J.R. Thompson, K. Stefansson, L.M. Roberts, U. Thorsteinsdottir, C.J. O'Donnell, R. McPherson, J. Erdmann, C.A. Consortium, N.J. Samani, Large-scale association analysis identifies 13 new susceptibility loci for coronary artery disease, Nat Genet. 43 (2011) 333–338.
[20] P. Deloukas, S. Kanoni, C. Willenborg, M. Farrall, T.L. Assimes, J.R. Thompson, E. Ingelsson, D. Saleheen, J. Erdmann, B.A. Goldstein, K. Stirrups, I.R. Konig, J.B. Cazier, A. Johansson, A.S. Hall, J.Y. Lee, C.J. Willer, J.C. Chambers, T. Esko, L. Folkersen, A. Goel, E. Grundberg, A.S. Havulinna, W.K. Ho, J.C. Hopewell, N. Eriksson, M.E. Kleber, K. Kristiansson, P. Lundmark, L.P. Lyytikainen, S. Rafelt, D. Shungin, R.J. Strawbridge, G. Thorleifsson, E. Tikkanen, N. Van Zuydam, B.F. Voight, L.L. Waite, W. Zhang, A. Ziegler, D. Absher, D. Altshuler, A.J. Balmforth, I. Barroso, P.S. Braund, C. Burgdorf, S. Claudi-Boehm, D. Cox, M. Dimitriou, R. Do, D. Consortium, C. Consortium, A.S. Doney, N. El Mokhtari, P. Eriksson, K. Fischer, P. Fontanillas, A. Franco-Cereceda, B. Gigante, L. Groop, S. Gustafsson, J. Hager, G. Hallmans, B.G. Han, S.E. Hunt, H.M. Kang, T. Illig, T. Kessler, J.W. Knowles, G. Kolovou, J. Kuusisto, C. Langenberg, C. Langford, K. Leander, M.L. Lokki, A. Lundmark, M.I. McCarthy, C. Meisinger, O. Melander, E. Mihailov, S. Maouche, A.D. Morris, M. Muller-Nurasyid, T.C. Mu, K. Nikus, J.F. Peden, N.W. Rayner, A. Rasheed, S. Rosinger, D. Rubin, M.P. Rumpf, A. Schafer, M. Sivananthan, C. Song, A.F. Stewart, S.T. Tan, G. Thorgeirsson, C.E. van der Schoot, P.J. Wagner, C. Wellcome Trust Case Control, G.A. Wells, P.S. Wild, T.P. Yang, P. Amouyel, D. Arveiler, H. Basart, M. Boehnke, E. Boerwinkle, P. Brambilla, F. Cambien, A.L. Cupples, U. de Faire, A. Dehghan, P. Diemert, S.E. Epstein, A. Evans, M.M. Ferrario, J. Ferrieres, D. Gauguier, A.S. Go, A.H. Goodall, V. Gudnason, S.L. Hazen, H. Holm, C. Iribarren, Y. Jang, M. Kahonen, F. Kee, H.S. Kim, N. Klopp, W. Koenig, W. Kratzer, K. Kuulasmaa, M. Laakso, R. Laaksonen, J.Y. Lee, L. Lind, W.H. Ouwehand, S. Parish, J.E. Park, N.L. Pedersen, A. Peters, T. Quertermous, D.J. Rader, V. Salomaa, E. Schadt, S.H. Shah, J. Sinisalo, K. Stark, K. Stefansson, D.A. Tregouet, J. Virtamo, L. Wallentin, N. Wareham, M.E. Zimmermann, M.S. Nieminen, C. Hengstenberg, M.S. Sandhu, T. Pastinen, A.C. Syvanen, G.K. Hovingh, G. Dedoussis, P.W. Franks, T. Lehtimaki, A. Metspalu, P.A. Zalloua, A. Siegbahn, S. Schreiber, S. Ripatti, S.S. Blankenberg, M. Perola, R. Clarke, B.O. Boehm, C. O'Donnell, M.P. Reilly, W. Marz, R. Collins, S. Kathiresan, A. Hamsten, J.S. Kooner, U. Thorsteinsdottir, J. Danesh, C.N. Palmer, R. Roberts, H. Watkins, H. Marz, N.J. Samani, Large-scale association analysis identifies new risk loci for coronary artery disease, Nat Genet. 45 (2013) 25–33.
[21] S. Duan, X. Luo, C. Dong, Identification of susceptibility modules for coronary artery disease using a genome wide integrated network analysis, Gene 531 (2) (2013) 347–354.
[22] N. Zhang, J.P. Sundberg, T. Gridley, Mice mutant for Ppap2c, a homolog of the germ cell migration regulator wunen, are viable and fertile, Genesis 27 (4) (2000) 137–140.
[23] J.L. Tomsig, A.H. Snyder, E.V. Berdyshev, A. Skobeleva, C. Mataya, V. Natarajan, D.N. Brindley, K.R. Lynch, Lipid phosphate phosphohydrolase type 1 (LPP1) degrades extracellular lysophosphatidic acid in vivo, Biochem. J. 419 (3) (2009) 611–618.
[24] N.S. Dhalla, Y.-J. Xu, S.-S. Sheu, P.S. Tappia, V. Panagia, Phosphatidic acid: a potential signal transducer for cardiac hypertrophy, J. Mol. Cell. Cardiol. 29 (11) (1997) 2865–2871.
[25] D. Shao, R. Tian, Glucose transporters in cardiac metabolism and hypertrophy, Compr. Physiol. 6 (1) (2015) 331–351.
[26] C.-C. Lin, C.-E. Lin, Y.-C. Lin, H. Lee, Lysophosphatidic acid induces reactive oxygen species generation through PLC/PKC/Nox pathway in PC-3 prostate cancer cells, FASEB J. 27 (1 Suppl.) (2013) S1144.5.
[27] C.-C. Lin, C.-E. Lin, Y.-C. Lin, H. Lee, Lysophosphatidic acid induces reactive oxygen species generation through protein kinase C in PC-3 prostate cancer cells, FASEB J. 26 (1 Suppl.) (2012) S657.13.
[28] I. Chatterjee, J. Baruah, E.E. Lurie, K.K. Wary, Endothelial lipid phosphate phosphatase-3 deficiency that disrupts the endothelial barrier function is a modifier of cardiovascular development, Cardiovasc Res. 111 (1) (2016) 105–118.
[29] K.E. Odening, M. Kirk, M. Brunner, O. Ziv, P. Lorvidhaya, G.X. Liu, L. Schofield, L. Chaves, X. Peng, M. Zehender, B.-R. Choi, G. Koren, Electrophysiological studies of transgenic long QT type 1 and type 2 rabbits reveal genotype-specific differences in ventricular refractoriness and His conduction, Am. J. Physiol. – Heart Circ. Physiol. 299 (3) (2010) H643–H655.
[30] S.-X. Zhou, J. Lei, C. Fang, Y.-L. Zhang, J.-F. Wang, Ventricular electrophysiology in congestive heart failure and its correlation with heart rate variability and baroreflex sensitivity: a canine model study, EP Eur. 11 (2) (2009) 245–251.
[31] Q. Zhou, T.J. Wang, C.T. Zhang, L. Ruan, L.D. Li, R.D. Xu, X.Q. Quan, M.K. Ni, [Effect of antiarrhythmic peptide on ventricular arrhythmia induced by lysophosphatidic acid], Zhonghua Xin Xue Guan Bing Za Zhi 39 (4) (2011) 301–304.